

# Fabrication of Graphene–Polyimide Nanocomposites with Superior Electrical Conductivity

Mitra Yoonessi,<sup>\*,†</sup> James R. Gaier,<sup>‡</sup> Muhammad Sahimi,<sup>§</sup> Tyrone L. Daulton,<sup>||</sup> Richard B. Kaner,<sup>†</sup> and Michael A. Meador<sup>‡</sup>

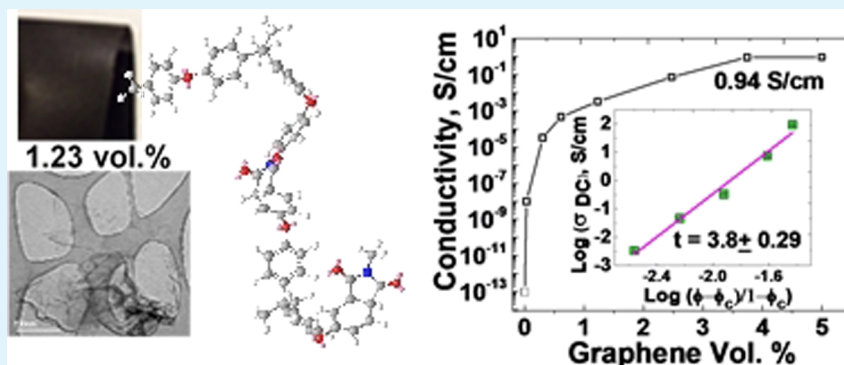
<sup>†</sup>Department of Chemistry and Biochemistry, University of California, Los Angeles, California 90095, United States

<sup>‡</sup>NASA Glenn Research Center, Cleveland, Ohio 44135, United States

<sup>§</sup>Department of Chemical Engineering and Materials Science, University of Southern California, Los Angeles, California 90089, United States

<sup>||</sup>Department of Physics, Institute for Materials Science & Engineering, Washington University in St. Louis, St. Louis, Missouri 63130, United States

## Supporting Information



**ABSTRACT:** We report on the fabrication of a novel class of lightweight materials, polyimide–graphene nanocomposites (0.01–5 vol %), with tunable electrical conductivity. The graphene–polyimide nanocomposites exhibit an ultra-low graphene percolation threshold of 0.03 vol % and maximum dc conductivity of 0.94 S/cm, which we attribute to excellent dispersion, extraordinary electron transport in the well-dispersed graphene, high number density of graphene nanosheets, and the  $\pi$ – $\pi$  interactions between the aromatic moieties of the polyimide and the carbon rings in graphene. The dc conductivity data are shown to follow the power-law dependence on the graphene volume fraction near the percolation threshold. The ac conductivity of the nanocomposites is accurately represented by the extended pair-approximation model. The exponent  $s$  of the approximation is estimated to be 0.45–0.61, indicating anomalous diffusion of charge particles and a fractal structure for the conducting phase, lending support to the percolation model. Low-temperature dc conductivity of the nanocomposites is well-approximated by the thermal fluctuation-induced tunneling. Wide-angle X-ray scattering and transmission electron microscopy were utilized to correlate the morphology with the electrical conductivity. The lack of maxima in X-ray indicates the loss of structural registry and short-range ordering.

**KEYWORDS:** graphene, polyimide, percolation, fluctuation-induced tunneling, nanocomposite

## 1. INTRODUCTION

Preparation of graphene with extraordinary properties, including ballistic charge-carrier transport, low-energy band  $\pi$  electrons, high thermal conductivity and stiffness, and excellent optical transparency perpendicular to the transmitted light, was first reported in 2004.<sup>1–7</sup> The material consists of freestanding hexagonal carbon nanosheets with a large surface area. Its conduction band, which is due to antibonding  $\pi^*$ , meets the valence band because of the  $\pi$  electrons at the Dirac point,<sup>1–4</sup> the six locations in the momentum space. Graphene has a charge carrier concentration of  $10^{13}$  that travels without scattering at room temperature and is only weakly temper-

ature-dependent.<sup>1–7</sup> It can be prepared from abundant natural graphite, and because its production is scalable, graphene offers an excellent low-cost material for various applications.<sup>8–13</sup> In particular, its exceptional electrical properties make it highly valuable for such applications as sensors, field-effect transistors, batteries, supercapacitors and electrostatic charge dissipation, conductive composites, and electromagnetic interference shielding when incorporated into the polymer matrix.<sup>8–13</sup>

Received: August 13, 2017

Accepted: November 23, 2017

Published: November 23, 2017

Polyimide resin is a class of versatile materials prepared by the condensation reaction with excellent properties, such as high thermal stability ( $T_g > 300$  °C) and thermal transition temperature ( $T_g > 200$  °C), low dielectric constant (~3.4), high tensile strength (~200 MPa), excellent dimensional stability, flexibility, and high UV and radiation resistance.<sup>14,15</sup> Their high-temperature properties are due to aromatic structure in the polymer backbone connected with the imide linkage that form the polymer's structure. Polyimide's exceptional properties along with the ability to operate in the broad temperature range of −270 to 400 °C makes it an ideal candidate material for such advanced technological applications as satellites and space structures, electronic packaging, and defense and aircraft components.<sup>14,15</sup>

Polyimide and other polymers are insulating with conductivity lower than  $10^{-13}$  S/cm, where the requirements are  $10^{-10}$  to  $10^{-12}$  S/cm for antistatic coating,  $10^{-7}$  to  $10^{-9}$  S/cm for static dissipative composites,  $10^{-3}$  to  $10^{-6}$  S/cm for conductive composites, and 1–100 S/cm for shielding composites.<sup>8–13</sup> Graphene has exceptional conductivity of  $5 \times 10^5$  S/cm because of high charge carrier density and charge carrier traveling without scattering in defect-free graphene nanosheets.<sup>1–3</sup> This excellent conductivity reaches a bulk value of metals with free valence electrons such as silver (Ag)  $6.3 \times 10^5$  S/cm, copper (Cu)  $5.96 \times 10^5$  S/cm, and gold (Au)  $4.1 \times 10^5$  S/cm.<sup>16</sup> Conductive polymers such as poly(3,4-ethylenedioxythiophene) (PEDOT) or polystyrene sulfone (PSS) have lower conductivity ranging up to  $1070 \pm 50$  S/cm where the electron transport is dominated by the hopping mechanism.<sup>17</sup> Defect-free graphene by chemical vapor deposition provides excellent materials for semiconductors with relatively high cost.<sup>18</sup> Recently, the physical vapor deposition method has been reported as an effective way to generate graphene with high electrical performance reaching nearly  $5 \times 10^5$  S/cm using amorphous carbon as a source and copper as a catalyst.<sup>19</sup>

Graphene-functionalized Ag hybrid nanofibers exhibited a high conductivity of 15 800 S/cm as flexible robust transistors for wearable electronics.<sup>20</sup> Conductive ink of graphene prepared under high shear rate turbulence flow condition in the presence of carboxymethylcellulose sodium salt showed a surface resistivity  $<2 \Omega/\square$ .<sup>21</sup> Sintering-free reactive organometallic silver ink formulation was developed using alcohol as a low-temperature reducing agent which exhibited a low resistivity ~39.2% compared to silver.<sup>22</sup> Composites of PEDOT:PSS with carboxylated carbon nanotubes used for ink jet printing showed a surface resistivity of  $1 \Omega/\square$  or lower.<sup>23</sup>

Many studies have been focused on the electrical properties of polymer–carbon nanomaterial nanocomposites targeting enhancements of their electrical properties.<sup>24–32</sup> Incorporation of carbon nanotubes in epoxy at the temperature range of 20–100 °C resulted in a percolation threshold of 0.04–2.5 wt % deduced from frequency-dependent response and a percolation of 0.3 wt % obtained from dc conductivity data.<sup>25</sup> Preparation of poly( $\epsilon$ -caprolactone)/multiwalled carbon nanotube nanocomposites resulted in a percolation level of 0.3 wt % from frequency-dependent ac conductivity where the electron transport mechanism was attributed to tunneling across insulating polymer boundaries.<sup>26</sup> Emulsion and suspension multiwall carbon nanotube polystyrene (PS) and polymethyl-metacrylate were prepared with percolation levels of 0.5–1.5 wt % for PS/MWCNT using sodium dodecyl sulfate as the surfactant.<sup>27</sup> Graphene's high aspect ratio and exceptional

electrical properties make it a valuable candidate for use in the fabrication of lightweight nanocomposites with tunable multifunctional properties reaching exceptionally high electrical conductivity.<sup>1–7,33</sup> We recently reported<sup>29</sup> fabrication of polycarbonate–graphene nanocomposites with a very low percolation threshold of 0.14 vol %, prepared by the emulsion method, reaching the highest dc conductivity of 0.51 S/cm at 2.2 vol % of graphene. A lower percolation threshold of 0.1 vol % was reported<sup>30</sup> for polystyrene–graphene nanocomposites, with a maximum conductivity of 0.001 S/cm at 1.0 vol %. Fabrication of polylactic acid-modified polystyrene–graphene nanocomposites resulted in a percolation threshold of 0.075 vol % and a conductivity of 0.0349 S/cm at 1.1 vol %. Octadecylamine (ODA)-treated graphene oxide–polystyrene possesses a percolation threshold of 0.45 vol % and a conductivity of  $4.6 \times 10^{-3}$  S/m with only 0.92 vol % of oxidized graphene (OG)–ODA in polystyrene.<sup>32</sup>

In this paper, we report on the fabrication of novel polyimide–graphene (PIG) nanocomposites with electrical properties that can be tuned by using reduced graphene nanosheets, ranging from the insulating regime below the percolation threshold to a maximum conductivity of 0.94 S/cm above the threshold. We have studied both dc and ac conductivities as well as low-temperature (90–273 K) dc conductivity of the nanocomposites to develop a comprehensive understanding of the percolation, conduction properties, and the electron transport mechanism in the nanocomposites. The low-temperature data might also be represented by the fluctuation-induced tunneling model, in which case one may conclude that electron transport occurs along the insulating interface and the polyimide chain segments that overcome temperature-dependent height of the voltage barrier. The dispersion and morphology of the graphene in polyimide was further examined using high-resolution transmission electron microscopy (HR-TEM) and wide-angle X-ray scattering (WAXS). The presence of expanded graphene clusters with high resin infusion well-dispersed in polyimide was confirmed by HR-TEM, where the loss of the structural registry and the absence of short-range ordering were indicated by the absence of maxima in the X-ray spectra.

## 2. RESULTS AND DISCUSSION

**2.1. Graphene.** Preparation of highly wrinkled exfoliated graphene nanosheets was reported recently<sup>10,11,33</sup> in which high thermal shock of acid-intercalated graphite was applied, with the estimated graphitic interlayer pressure exceeding the calculated van der Waals binding forces between the nanosheets in the graphite crystalline structure. Aksay et al.<sup>33</sup> reported the required pressure for separating the OG nanosheets to be 2.5 MPa, which is at least 1 order of magnitude larger than the estimated van der Waals force. During the process, the reaction time should be shorter than the diffusion time scale to avoid slow gas diffusion through the lateral dimension of the graphitic interlayer.<sup>10,11,33</sup> This results in exfoliated graphene nanosheets with an extreme topology that have epoxide, hydroxyl, and carboxylic groups. The graphene nanosheets shown in Figure 1a,b exhibit high transparency with respect to the electron beam in the perpendicular direction, which is indicative of the possibility of the existence of a single graphene sheet. The lateral dimension was measured to vary between 700 nm and 15  $\mu$ m without taking into account the large height and folding, reported due to the 5–8–5 configurational rearrangement of

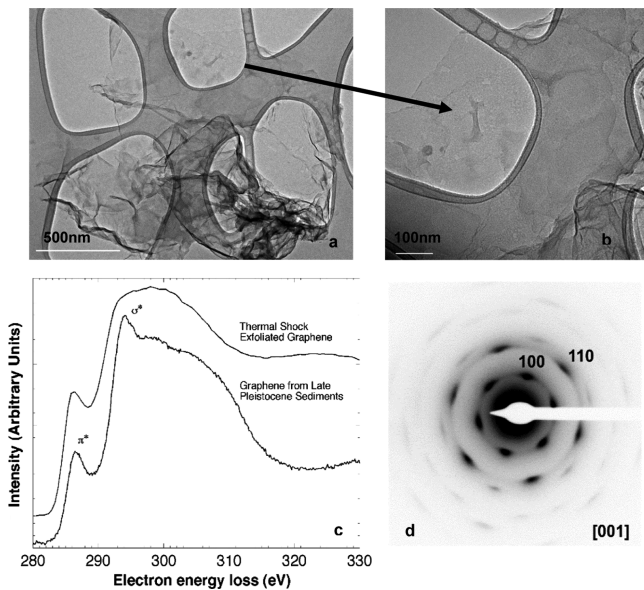


**Figure 1.** Transmission electron micrograph of the reduced graphene. (a) Nearly transparent sheet with wrinkling and folding that appears as an elevated height, (b) defect sites in the single graphene sheet, (c) EELS spectra of the C–K absorption edge of the thermal shock exfoliated graphene used in preparing nanocomposites is compared to the spectra from natural polycrystalline aggregates of single sheet graphene, and (d) representative [001] zone axis diffraction pattern from exfoliated graphene. For clarity, the pattern is displayed in reverse image contrast.

hexagonal carbon rings.<sup>10,11,29,33</sup> The Brunauer–Emmett–Teller method was used to measure the surface area and was estimated to be  $1150 \pm 75 \text{ m}^2/\text{g}$ , which should be compared with the theoretical estimate of  $2630 \text{ m}^2/\text{g}$ .<sup>1–4</sup>

The C–K absorption edge of exfoliated graphene was measured using electron energy loss spectroscopy (EELS), Figure 1c. Absorption edges result from core level ionization by the incident electron beam and provide information on the electronic bonding structure of atoms of an analyzed element. The exfoliated graphene notably lacks a sharp  $\sigma^*$  peak at  $\sim 294 \text{ eV}$  (corresponding to transitions from the 1s to  $\sigma^*$  states), as observed in natural graphene.<sup>34</sup> The exfoliated graphene instead displays a broader peak between 290 and 310 eV similar to the spectra from amorphous carbon, suggesting the presence of high density of atomic defects. Electron diffraction from the [001] zone axis of exfoliated graphene (Figure 1d) displays broad Bragg reflections and diffuse intensity indicative of atomic disorder within the sheets. In comparison, the graphene sheets synthesized in the gas phase<sup>35</sup> were reported to be defect-free based on electron diffraction patterns that exhibited sharp, circular Bragg spots and lack diffuse intensity, similar to patterns obtained from well-ordered graphene sheets produced by micromechanical cleavage.

The EELS spectra of the exfoliated graphene also display an O–K absorption edge. Ratios of the background-subtracted C and O EELS core-loss signal were converted to atomic ratios using partial cross sections calculated from theoretical Hartree–Slater models. The oxygen concentration in the exfoliated graphene was estimated at  $\sim 6 \text{ at. \%}$ . The presence of O is consistent with the attached epoxide, hydroxyl, and carboxylic groups, and their attachment could be accommodated by the atomic disorder present in the sheets.

**2.2. Graphene–Polyimide Nanocomposites.** Graphene dispersion influences strongly the properties of polymer nanocomposites by increasing the surface-to-volume ratio and the available interfacial area that interacts with the polymer's chains.<sup>36–40</sup> Novel properties can be obtained by tailoring the dispersion, the size of the nanoparticles and their aspect ratio, the surface chemistry, the polymer chain length, and tuning and controlling the interactions of the nanoparticle surface with the polymer chains. The dispersion may be defined over different length scales as short-range particle–particle interactions and long-range particle ordering.<sup>36</sup> Theoretical modeling of mica-filled polymer melt predicted that a combination of energetic and entropic factors determines the ordering or loss of structural registry of the nanocomposite.<sup>36–39</sup> Studies of short-range dispersion using high-resolution microscopy, as well as probing montmorillonite clay at different length scales using small-angle neutron scattering, have been carried out.<sup>37</sup>

Aromatic polyimides with high thermal stability, low color, flexibility, radiation resistance, and excellent performance over the temperature range of  $65\text{--}357^\circ\text{C}$  are suitable for many advanced technological applications. We previously reported<sup>14</sup> synthesis of polyimide with ether and bisphenol linkage in the backbone, as shown in Figure 2, which imparts more flexibility and solubility to the polyimide.<sup>14</sup> Enhancements of thermal, mechanical, and high-temperature shape memory effects were demonstrated in the PIG nanocomposites.

Hereafter, when we refer to the graphene content of the nanocomposites, we mean its volume percentage in the material. We fabricated a series of PIG nanocomposite thin films with a graphene content of 0.015–5% and a thickness of 150–200  $\mu\text{m}$ , to tune their electrical properties, using well-dispersed reduced sp<sup>2</sup>-hybridized graphene. The PIG films were prepared by co-mixing of the well-dispersed graphene in an N-methyl-2-pyrrolidone + polyimide solution, followed by solvent removal (Supporting Information). We then focused on changing the dc and ac electrical conductivity of the nanocomposite as a function of the graphene content, as well as understanding the governing conduction mechanism and how it correlates with the dispersion in the polyimide resin matrix.

**2.3. dc Conductivity.** Figure 3 presents the dc conductivity of the PIG nanocomposites (see also the Supporting Information). At extremely low graphene contents, the material is essentially insulating. However, its dc conductivity increases with increasing graphene content. The dc conductivities

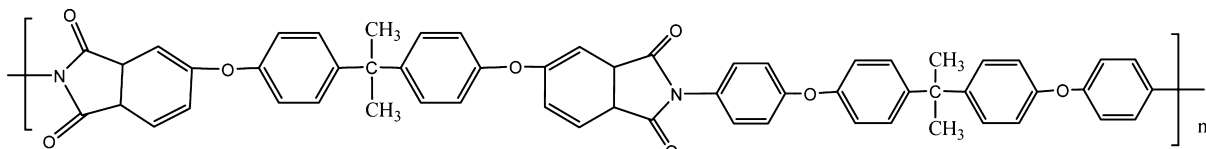


**Figure 2.** Chemical structure of polyimide.

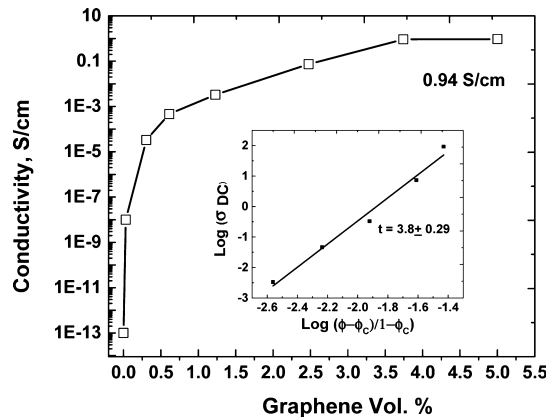


**Figure 3.** dc conductivity of the polyimide–graphene nanocomposites. The inset shows fit of the data to eq 1, the power law predicted by the percolation theory.

reported herein are the measured *in-plane* conductivities of the films. The films were polished before the electrical conductivity measurement to remove any processing-induced morphology surface features. Overall, the high aspect ratio of the graphene induces some degree of planar orientation resulting in much lower *through-plane* conductivity. We studied this matter extensively in our previous reports,<sup>40</sup> where we used nickel-tethered graphene to generate PIG nanocomposite films with *through-plane* insulation and excellent *in-plane* conductivity. When the graphene volume fraction reaches its percolation threshold, the overall conductivity exhibits a sudden increase. We define the percolation conductivity threshold<sup>40–44</sup> as the volume percent of the graphene in the nanocomposite at which onset of a sudden “phase transition” occurs, whereby the nanocomposite changes from an insulating material to a conductive one. The change occurs when the conductive particles—graphene in this case—are in close proximity, allowing charge transfer directly or through overcoming the energy barrier across insulating polymer chains that occur forming a sample-spanning cluster across the nanocomposite, hence allowing electron or charge-carrier transport. Different electron transport mechanisms including hoping and tunneling have been attributed to the electron transport where we describe tunneling between the graphene nanosheets shortly. The percolation threshold is related not only to the nanoparticle volume fraction but also their orientation, the extent of their dispersion and aggregation, their aspect ratio and interfacial area with the polymeric matrix, and the physics of charge-carrier transport in the material such as electron hopping and/or tunneling. Percolation theory<sup>41–43</sup> predicts that, near the percolation threshold or critical volume fraction  $\phi_c$  of graphene, the dc electrical conductivity  $\sigma_{dc}$  of the nanocomposite follows a power law<sup>21,22,41–43</sup>

$$\sigma_{dc} = \sigma_f [(\phi - \phi_c)/(1 - \phi_c)]^t \quad (1)$$

where  $t$  is called the *conductivity exponent* and  $\sigma_f$  is the nanoparticle conductivity. The conductivity exponent  $t$  is often universal, taking on a value that depends only on the dimensionality of the material and not the details of its morphology. Its universal value for three-dimensional materials is about 2.<sup>43</sup> Under certain circumstances,<sup>45,46</sup> however, the exponent  $t$  may be nonuniversal and is influenced by the spatial distribution of the conductivity of the local conduction channels in the material. For such materials, the conductivity

exponent is anywhere between 2 and 5,<sup>46</sup> which is in agreement with what we report here for our nanocomposites and what we describe and discuss below.

Figure 3 indicates that the percolation transition to a conducting nanocomposite occurs at a graphene content of 0.03%, with the maximum conductivity reaching 0.94 S/cm achieved at higher graphene volume fractions (5%). The percolation threshold  $\phi_c$  is much lower than the 17% theoretical volume fraction predicted<sup>41,42</sup> for completely random composites. This can be attributed to a variety of factors including extreme high aspect ratio of graphene, high charge transport on the sp<sup>2</sup>-hybridized graphene, high particle number density of graphene per unit volume, excellent dispersion of graphene in the polyimide resin matrix, and short-range interactions of the graphene nanoparticles within the polyimide resin matrix. The enhanced interactions between the  $\pi-\pi^*$  electron cloud of graphene and  $\pi$  electrons of aromatic benzene rings may also contribute to the increased electrical conductivity of the nanocomposites. The enhanced interaction of aromatic moieties, such as pyrene, with graphitic structures have been widely studied and reported.<sup>47,48</sup>

If we fit the dc conductivity data to the power law 1, we obtain  $\sigma_f = 10^{5.12 \pm 0.57}$  S/cm and a conductivity exponent,  $t = 3.8 \pm 0.2$ . The goodness of the fit,  $R^2$ , is 0.991. It should be instructive to compare our estimate of  $t$  with those of other nanocomposites. Our previous studies of conduction in solution-processed reduced graphene-polycarbonate nanocomposites resulted<sup>29</sup> in a comparable conductivity exponent,  $t = 4.04 \pm 0.58$ , while an estimate of 3.3 was obtained for the graphene–hydrogel system.<sup>49</sup> Incorporating graphene in urethane acrylate resulted in a percolation volume fraction of 0.07% and a conductivity exponent of around 5.<sup>50</sup> A lower value of 2.53 for the conductivity exponent and a very low percolation threshold of 0.033% were recently reported for the graphene–gelatin nanocomposite.<sup>51</sup> The percolation threshold of the polystyrene–graphene nanocomposites was reported to be at the graphene content of 0.1%; that of polylactic acid-modified graphene–polystyrene nanocomposites was recently estimated to be 0.075%,<sup>31</sup> whereas percolation thresholds of 0.14 and 0.37% was reported for reduced graphene–polycarbonate, fabricated by solution blending and emulsion mixing methods.<sup>29</sup> Nanocomposites that consisted of polystyrene and chemically-converted graphene possess a maximum conductivity of 0.72 S/cm at a graphene content of 2.45% with a very low percolation of 0.19%.<sup>30</sup>

Using a tunneling percolation and Monte Carlo simulations, the resistivity of graphene-based nanocomposites predicted an inverse power-law dependence of resistivity and volume fraction near the percolation threshold.<sup>52</sup> This study predicted higher sensitivity to the aspect ratio near percolation, especially at the lower particle number density.<sup>53</sup> Theoretical studies proposed an inverse relationship of the aspect ratio and critical volume fraction, where the excluded volume fraction of the oblate structure was taken into account.<sup>52–54</sup> Monte Carlo simulations predicted that the degree of contact network is the coordination number  $\langle z \rangle$  with a minimum for spherical and increasing with shape anisotropy for rod and disk shapes. This also related to weak entropic forces at the polymer nanoparticle interfaces and the tendency of the nanostructured materials to aggregate and agglomerate.<sup>54</sup> At the low concentrations of disk-shaped structures, the  $\langle z \rangle$  approximated as ~1.<sup>52–54</sup> Therefore, the aspect ratio, AR, =  $D/l$  is related to the percolation volume

fraction roughly as  $(D/l)\phi_c \approx 1$ , for conductive particles when dispersed as single particles or stacked without aggregation and clustering.<sup>41–44,52–54</sup> Here,  $D$  is the average diameter of the graphene nanosheets and  $l$  is the average thickness of the stacks. If we assume that the graphene films are monotonically thin, then the above correlation predicts an estimated aspect ratio of  $\sim 3333$  and a graphene lateral dimension of  $1.12\text{ }\mu\text{m}$ . The average graphene diameter calculated and measured by electron microscopy is about  $3\text{ }\mu\text{m}$ .<sup>21</sup> If stacking is taken into account, the same approximation predicts an average graphene stack thickness of about  $9\text{ \AA}$ , which represents graphene stacks consisting of an average of about 2.6 layers of graphene.

**2.4. Morphology.** WAXS spectra of the PIG nanocomposites exhibits a maximum at a  $2\theta$  value of  $17.4^\circ$  with  $d = 5.092\text{ \AA}$  corresponding to the amorphous peak of polyimide. This is shown in Figure 4. No peak corresponding to the  $3.354\text{ \AA}$

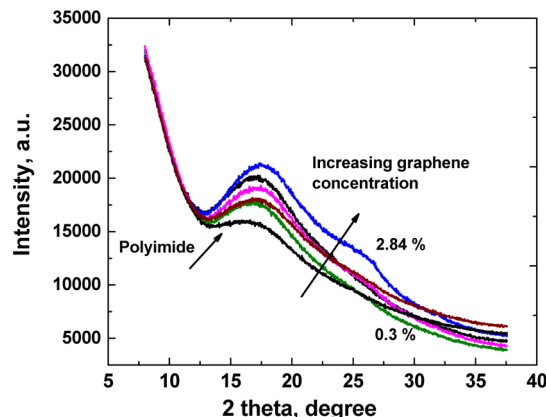


**Figure 4.** WAXS of graphene in the polyimide resin matrix with the graphene content ranging from 0 to 2.84%. The maximum at  $d = 5.092\text{ \AA}$  corresponds to amorphous polyimide resin (black line), whereas no peak at  $3.354\text{ \AA}$  is seen for the graphene content of up to 2.84% (blue line).

$\text{\AA}$  of the graphene stacking is observed up to the graphene volume percent of 3.74% and higher, where a broad low-intensity shoulder peak appears. This indicates excellent dispersion of graphene in the nanocomposite with low graphene content and the presence of some graphene stacks at the higher graphene contents.

**2.5. High-Resolution TEM.** The extent of graphene dispersion and aggregation in the polyimide resin was investigated using (HR)-TEM. Figures 5a–c are the low magnification micrographs showing the dispersion of the graphene layers and stacks in the nanocomposite with graphene contents of 0.3 and 1.23%, respectively. High particle number density of the graphene layers and stacks are observed in both nanocomposites. The composite with 0.3% graphene, which is above the percolation threshold, has an electrical conductivity of  $3.35 \times 10^{-5}\text{ S/cm}$ . Figure 5d shows expanded structure of graphene clusters with long-range interactions. Figure 5a demonstrates expanded and disordered structures of graphene layers and stacks with onset of network formation. These nanosheets and stacks are in close proximity yet. Short-range correlations between graphene stacks exist, and the distance between the graphene nanosheets appears to be less than the size of the graphene. The nanocomposite with the graphene content of 1.23% has a conductivity of  $0.003\text{ S/cm}$  in the plateau regime with an Ohmic conductivity, where charge

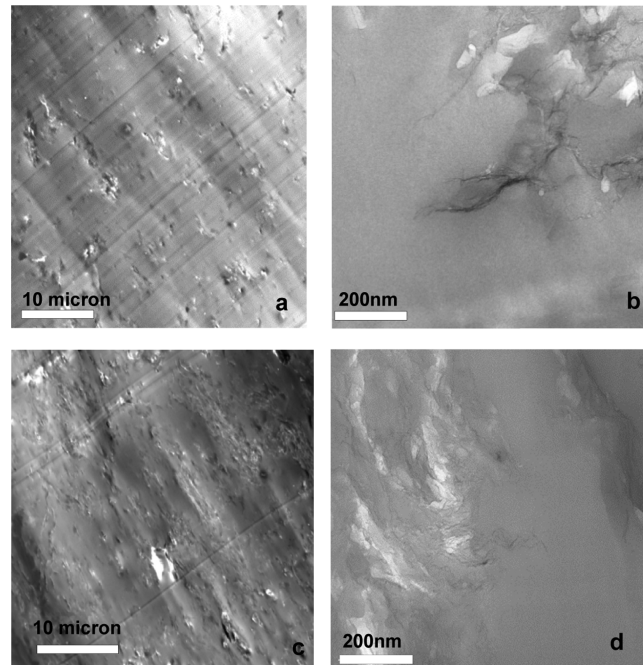


**Figure 5.** Transmission electron micrograph of the polyimide nanocomposite nanocomposites, 0.3% (a,b) and 1.23% (c,d). (a,c) exhibit a lower magnification to demonstrate the local dispersion of the graphene nanosheets and expanded graphene clusters and fractal structures in the polyimide resin matrix. (b,d) show a higher magnification of the same area to exhibit the graphene nanosheet morphology and infusion of polyimide resin in between graphene expanded structures.

transport is frequency-independent, when measured using ac conductivity. A high particle number density of graphene in the polyimide resin matrix is evident in the TEM micrograph. The particles appear to form a fractal structure, as they are in very close proximity, or connected altogether, hence allowing charge transport through the nanosheets and with a minimal distance between the sheets. This also supports the percolation model. This matter is investigated using ac conductivity which will be discussed next.

**2.6. Temperature-Dependence of dc Conductivity.** In an attempt to better understand the governing mechanisms of electrical conduction in the nanocomposites at higher graphene contents, low-temperature dc conductivity of polyimide graphene nanocomposite with graphene volume fractions larger than the percolation threshold was studied. Figure 6 shows temperature-dependence of the measured conductivities with graphene contents of 3.74 and 5%, with the temperature range well below the polyimide alpha and beta thermal transition temperatures. The conductivities increase with increasing temperature, with the rate of conductivity change with temperature,  $d\sigma/dT$ , being higher for the 5% graphene content.

The PIG nanocomposites are disordered heterogeneous materials that consist of two phases (graphene and polyimide) with extremely large interfacial areas of graphene covered by polyimide, where the graphene or its stacks are separated by the polyimide resin matrix. The aforementioned thickness and lateral dimensions of the graphene stacks suggest that the available interfacial area is lower than that of monodispersed graphene nanosheets in the matrix. The separation distance between graphene nanosheets is linked to their short-range interactions. At or above the percolation threshold, the distance

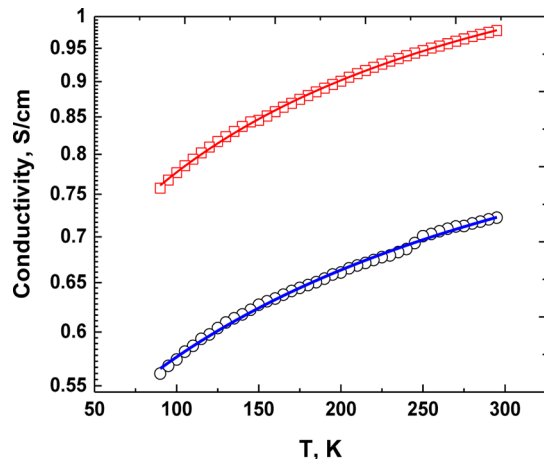


**Figure 6.** Temperature-dependence of the dc conductivity of the nanocomposites with graphene contents of 3.74% (○) and 5% (□). Solid curves represent the predictions of the fluctuation-induced tunneling model.

between the conductive graphene stacks become finite and attains a minimum where the conductive particles are in close proximity or particle–particle contacts exist. Upon application of a voltage, the charge carriers move in the conductive graphene, encountering a potential barrier because of the presence of the polyimide interface and insulating polyimide between the conductive graphene sheets. When the potential is high enough, the charge carrier overcomes the voltage barrier and travels through the insulating interface through the polyimide chain segments.<sup>41–44,55</sup>

The dc conductivity of the graphene–polyimide nanocomposites with graphene contents of 3.74 and 5% increases with increasing temperature, indicating that the height of the voltage barrier can fluctuate with thermal energy and being of thermally-assisted charge transfer.<sup>52</sup> In this approximation, modulating the effects of thermally-activated voltage fluctuation with various heights of the potential barrier induced by local temperature fluctuation is taken into account<sup>52–54</sup>

$$\sigma \approx \exp[-T_1/(T + T_0)] \quad (2)$$

where

$$T_1 = \frac{wA\epsilon^2}{8\pi k} \quad (3)$$

$$T_0 = \frac{2T_1}{\pi w \chi} \quad (4)$$

$$\chi = \left( \frac{2mV_0}{h^2} \right)^{1/2} \quad (5)$$

$$\epsilon = \frac{4V_0}{ew} \quad (6)$$

with  $T_1$  and  $T_0$  being constant temperatures related to the thermal energy required to overcome the potential barrier.<sup>55–57</sup> Here,  $k$  is the Boltzmann's constant,  $m$  and  $e$  are electron mass and charge,  $V_0$  is the potential barrier height,  $w$  is the average interparticle (graphene) distance, and  $A$  is the area of the capacitance formed.  $T_0$  is the temperature above which the thermal effects must be considered, whereas  $T_1$  determines the shape of the voltage barrier function.<sup>55</sup>

The temperature-dependence of the dc conductivity with graphene contents of 3.74 and 5% is compared with the fluctuation-induced tunneling model in Figure 6. The approximation yields estimates for  $T_1$  and  $T_0$ , which are 228 and 231 K for the 3.74% nanocomposite and 179 and 125.7 K for the 5% graphene nanocomposite. The two constants are significantly lower for the 5% nanocomposite, indicating weaker temperature-dependence when the graphene content is higher. In addition, with higher graphene content the separation distance between the particles decreases and results in a lower energy barrier for charge transport. Indeed,  $kT_1$  is about  $1.96 \times 10^{-2}$  eV for the graphene content of 3.74%, whereas it is  $1.54 \times 10^{-2}$  eV for the 5% nanocomposite.

Given the accuracy of the tunneling model and the equally accurate percolation model, the question that arises is: what is the mechanism of conduction in the PIG nanocomposites? If the percolation model is applicable, it implies that conduction is through the sample-spanning conducting phase of the nanocomposite. On the other hand, if tunneling electron transport occurs along the insulating polymer chain in a homogeneously dispersed conductive graphene sheets in the matrix, then it is straightforward to show, based on eqs 2–6, that at a constant temperature a plot of  $\log(\sigma)$  versus  $\phi^{-1/3}$  should be linear.<sup>55–57</sup> Figure 7 shows such a plot of our data for the graphene content

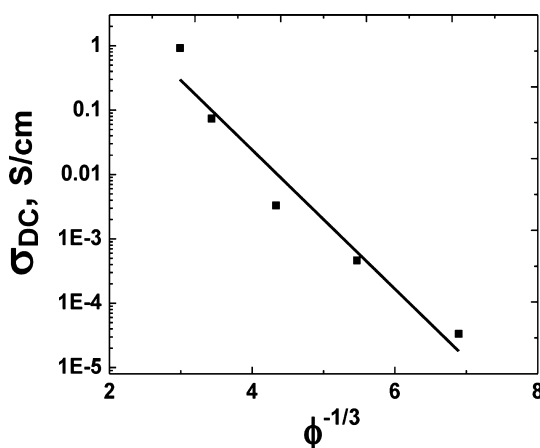


**Figure 7.** Plot of  $\log(\text{dc conductivity})$  vs  $\phi^{-1/3}$ .

of 0.3–3.74%. There is noticeable departure from linearity at a high graphene content of 3.74%, which is the regime in which the graphene particles are in physical contact. In addition, although the goodness fit,  $R^2$ , is 0.93, there is still noticeable deviation from the straight line at high graphene contents. It is, of course, possible that the tunneling model is applicable at very low graphene contents, but the percolation model describes the data when the graphene phase forms a sample-spanning cluster. In other words, there is no single model that can explain all the data. Thus, the matter requires further investigation.

**2.7. Broadband ac Spectroscopy.** To further study the issue, we carried out measurements of the ac conductivity. Figure 8 presents the frequency-dependence of the real part of the complex ac conductivity of the PIG nanocomposites with graphene contents of 0.3, 0.6, 1.23, 2.48, 3.74, and 5.0%, indicating that the ac conductivity is independent of the frequency for the graphene contents of 2.48, 3.74, and 5%, which are well above the percolation threshold. This indicates that the charge carrier density is high enough and travels fast through the nanocomposite matrix that even at high

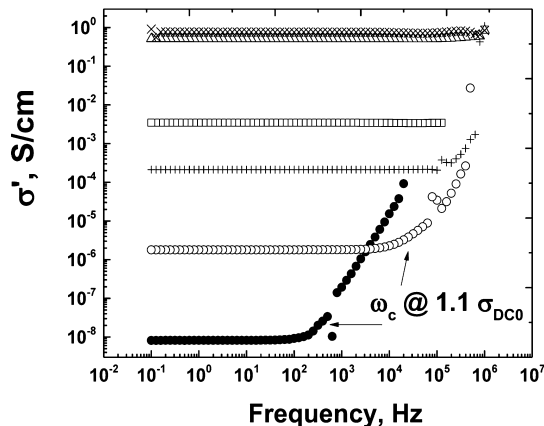


**Figure 8.** Real part of the complex ac conductivity ( $\sigma'$ ) vs frequency with graphene volume fractions of 0.3 (●), 0.6 (○), 1.23 (+), 2.48 (□), 3.74 (Δ), and 5 (×).

frequencies the current and voltage are in phase with no lag between them, that is, zero phase angle. On the other hand, the ac conductivity with graphene contents of 0.6 and 0.3% is independent of the frequency, followed by a regime in which the conductivity depends on the frequency. The charge carriers can travel throughout the nanocomposite matrix at lower frequencies, but there is a lag at higher frequencies (nonzero phase angle). This may be attributed to the lower density of the charge carriers at lower volume fractions and in the presence of insulating interfacial polymer barrier between the graphene particles. The real component of conductivity is independent of the frequency, until a critical frequency  $\omega_c$ , estimated to be at  $1.1\sigma_{dc0}$ .<sup>41,58–60</sup> When the graphene content is 1.23%, the conductivity depends weakly on the frequency only at higher values.

The experimental data may be fit to the extended pair-approximation model<sup>60</sup>

$$\sigma(\omega)/\sigma_{dc0} = 1 + k(\omega/\omega_c)^s \quad (7)$$

in which  $k$  and  $s$  are fitting parameters. Fitting the experimental data with the extended pair-approximation model yields estimates of  $s$  that are 0.5, 0.65, and 0.45 for the graphene contents of 0.3, 0.6, and 1.23%, respectively. The estimates, along with the values of the critical frequency are listed in Table 1. For insulating polymers,  $s = 1$ ; hopping conduction in

**Table 1. Real Component of ac Conductivity, Critical Frequency, and  $s$  for the 0.3, 0.6, and 1.23% Graphene–Polyimide Nanocomposites**

vol %	$\sigma_{dc0}$ S/cm	$\omega_c$ Hz	$s$
0.3	$8.2 \times 10^{-9}$	150.47	0.5
0.6	$1.88 \times 10^{-6}$	$7.0 \times 10^3$	0.65
1.23	$2.0 \times 10^{-4}$	$1.24 \times 10^5$	0.45

disordered materials is associated with  $0.8 < s < 1.0$ , while  $s \approx 0.6$  is obtained for the conductivity of fractal clusters in which anomalous diffusion—one in which the mean-square displacements grow with time more slowly than linearly—takes place.<sup>55,59,60</sup> Thus, the PIG nanocomposites yielding  $s \approx 0.44$ –0.6 implies that the graphene phase of the composites has a fractal structure in the polyimide resin matrix, lending support to the percolation model, because the sample-spanning conduction cluster at or very close to the percolation threshold

is also a fractal cluster.<sup>41–46</sup> Moreover, our estimates of  $s$  suggest that, even though the graphene nanosheets are inherently two dimensional, they form a three-dimensional fractal structure in the nanocomposites when stacked together and dispersed in the three-dimensional polyimide resin matrix. The fractal structure is characterized by a correlation length  $\xi$ , such that below the critical frequency  $\omega_c$ , the charge carrier can travel distances much larger than  $\xi$ , but when the critical frequency is reached, such travels are no longer possible.<sup>41–43</sup> In that case, the power-law dependence of the conductivity on the frequency emerges, with the aforementioned values of the exponent  $s$ . The values of the exponent  $s$  and the critical frequency  $\omega_c$  are listed in Table 1.

### 3. CONCLUSIONS

A series of polyimide–graphene nanocomposites with a range of electrical conductivity and a low graphene percolation threshold of 0.03 vol % was fabricated. The electrical performance of nanocomposites is tunable through the volume fraction of graphene and reaches a maximum of 0.94 S/cm. The ac conductivity data exhibited a frequency-independent behavior when the graphene content is larger than 1.23%. The low percolation threshold and high maximum dc conductivity are attributed to the excellent dispersion of graphene in the polyimide resin and favorable interactions between the polyimide aromatic structure and the electron cloud in the graphene. Fit of the ac conductivity data with the universal extended pair-approximation model yielded values of the  $s$  exponent of the model that indicates a fractal structure for the graphene phase. Low-temperature dc conductivity data of the nanocomposites exhibited temperature-dependence that is well-represented by the fluctuation-induced tunneling model. The absence of maxima in the WAXS spectra indicates a disordered structure in terms of short-range ordering of the graphene in the nanocomposites. The spectrum of the nanocomposite with a graphene content of 2.84% exhibits a very broad shoulder that emerges at 3.35 Å. High-resolution TEM provides evidence for a well-dispersed resin-infused graphene layers and stacks, in agreement with a fractal structure.

### ASSOCIATED CONTENT

#### Supporting Information

The Supporting Information is available free of charge on the ACS Publications website at DOI: [10.1021/acsami.7b12104](https://doi.org/10.1021/acsami.7b12104).

Detailed materials and preparation methods of graphene–polyimide nanocomposite films; characterization and testing methods; and schematics of the four-point electrical conductivity measurements at liquid He temperature in vacuum (PDF)

### AUTHOR INFORMATION

#### Corresponding Author

\*E-mail: [mitra.yoonessi@gmail.com](mailto:mitra.yoonessi@gmail.com).

#### ORCID

Mitra Yoonessi: [0000-0002-0078-8999](https://orcid.org/0000-0002-0078-8999)

Muhammad Sahimi: [0000-0002-8009-542X](https://orcid.org/0000-0002-8009-542X)

Richard B. Kaner: [0000-0003-0345-4924](https://orcid.org/0000-0003-0345-4924)

#### Notes

The authors declare no competing financial interest.

## ACKNOWLEDGMENTS

Funding for this work was provided by the Subsonic Fixed Wing Project, Fundamental Aeronautics Program under NASA Contract NNC07BA13B. Dr. Francisco Sola of NASA Glenn Research Center and Dr. Volker Strauss, University of California, Los Angeles are thanked for helpful discussions and support.

## REFERENCES

- (1) Geim, A. K. Graphene: Status and Prospects. *Science* **2009**, *324*, 1530–1534.
- (2) Geim, A. K.; Novoselov, K. S. The Rise of Graphene. *Nat. Mater.* **2007**, *6*, 183–191.
- (3) Li, D.; Kaner, R. B. Graphene-Based Materials. *Science* **2008**, *320*, 1170–1171.
- (4) Katsnelson, M. I.; Geim, A. K. Electron Scattering on Microscopic Corrugations in Graphene. *Philos. Trans. R. Soc., A* **2008**, *366*, 195–204.
- (5) Zhu, Y.; Murali, S.; Cai, W.; Li, X.; Suk, J. W.; Potts, J. R.; Ruoff, R. S. Graphene and Graphene Oxide: Synthesis, Properties, and Applications. *Adv. Mater.* **2010**, *22*, 3906–3924.
- (6) Allen, M. J.; Tung, V. C.; Kaner, R. B. Honeycomb Carbon: A Review of Graphene. *Chem. Rev.* **2010**, *110*, 132–145.
- (7) Geim, A. K. Random Walk to Graphene (Nobel Lecture). *Angew. Chem., Int. Ed.* **2011**, *50*, 6966–6985.
- (8) El-Kady, M. F.; Kaner, R. B. Scalable fabrication of high-power graphene micro-supercapacitors for flexible and on-chip energy storage. *Nat. Commun.* **2013**, *4*, 1475.
- (9) El-Kady, M. F.; Strong, V.; Dubin, S.; Kaner, R. B. Laser Scribing of High-Performance and Flexible Graphene-Based Electrochemical Capacitors. *Science* **2012**, *335*, 1326–1330.
- (10) Schniepp, H. C.; Kudin, K. N.; Li, J.-L.; Prud'homme, R. K.; Car, R.; Saville, D. A.; Aksay, I. A. Bending Properties of Single Functionalized Graphene Sheets Probed by Atomic Force Microscopy. *ACS Nano* **2008**, *2*, 2577–2584.
- (11) Schniepp, H. C.; Li, J.-L.; McAllister, M. J.; Sai, H.; Herrero-Alonso, M.; Adamson, D. H.; Prud'homme, R. K.; Car, R.; Saville, D. A.; Aksay, I. A. Functionalized Single Graphene Sheets Derived from Splitting Graphite Oxide. *J. Phys. Chem. B* **2006**, *110*, 8535–8539.
- (12) Yang, Y.; Kaner, R. B.; Tung, C.-C.; Allen, M. High-Throughput Solution Processing of Large Scale Graphene and Device Application. U.S. Patent 9,105,403 B2, Aug 11, 2015.
- (13) Paton, K. R.; Varrla, E.; Backes, C.; Smith, R. J.; Khan, U.; O'Neill, A.; Boland, C.; Lotya, M.; Istrate, O. M.; King, P.; Higgins, T.; Barwick, S.; May, P.; Puczkarski, P.; Ahmed, I.; Moebius, M.; Pettersson, H.; Long, E.; Coelho, J.; O'Brien, S. E.; McGuire, E. K.; Sanchez, B. M.; Duesberg, G. S.; McEvoy, N.; Pennycook, T. J.; Downing, C.; Crossley, A.; Nicolosi, V.; Coleman, J. N. Scalable Production of Large Quantities of Defect-Free Few-Layer Graphene by Shear Exfoliation in Liquids. *Nat. Mater.* **2014**, *13*, 624–630.
- (14) Yoonessi, M.; Shi, Y.; Scheiman, D. A.; Lebron-Colon, M.; Tigelaar, D. M.; Weiss, R. A.; Meador, M. A. Graphene Polyimide Nanocomposites: Thermal, Mechanical, and High-Temperature Shape Memory Effects. *ACS Nano* **2012**, *6*, 7644–7655.
- (15) Wilson, D.; Stenzenberger, H. D.; Hergenrother, P. M. *Polyimides*; Springer: Berlin, Germany, 1990.
- (16) Mittemeijer, E. J. *Fundamentals of Materials Science*; Springer-Verlag GmbH: Berlin, Germany, 2011.
- (17) Tait, J. G.; Worfolk, B. J.; Maloney, S. A.; Hauger, T. C.; Elias, A. L.; Buriak, J. M.; Harris, K. D. Spray Coated High-Conductivity PEDOT:PSS Transparent Electrodes for Stretchable and Mechanically-Robust Organic Solar Cells. *Sol. Energy Mater. Sol. Cells* **2013**, *110*, 98–106.
- (18) Li, X.; Cai, W.; An, J.; Kim, S.; Nah, J.; Yang, D.; Piner, R.; Velamakanni, A.; Jung, I.; Tutuc, E.; Banerjee, S. K.; Colombo, L.; Ruoff, R. S. Large-Area Synthesis of High-Quality and Uniform Graphene Films on Copper Foils. *Science* **2009**, *324*, 1312–1314.
- (19) Narula, U.; Tan, C. M.; Lai, C. S. Growth Mechanism for Low Temperature PVD Graphene Synthesis on Copper Using Amorphous Carbon. *Sci. Rep.* **2017**, *7*, 44112.
- (20) Yoon, S. S.; Lee, K. E.; Cha, H.-J.; Seong, D. G.; Um, M.-K.; Byun, J.-H.; Oh, Y.; Oh, J. H.; Lee, W.; Lee, J. U. Highly Conductive Graphene/Ag Hybrid Fibers for Flexible Fiber-Type Transistors. *Sci. Rep.* **2015**, *5*, 6366.
- (21) Karagiannidis, P. G.; Hodge, S. A.; Lombardi, L.; Tomarchio, F.; Decorde, N.; Milana, S.; Goykhman, I.; Su, Y.; Mesite, S. V.; Johnstone, D. N.; Leary, R. K.; Midgley, P. A.; Pugno, N. M.; Torrisi, F.; Ferrari, A. C. Microfluidization of Graphite and Formulation of Graphene-Based Conductive Inks. *ACS Nano* **2017**, *11*, 2742–2755.
- (22) Black, K.; Singh, J.; Mehta, D.; Sung, S.; Sutcliffe, C. J.; Chalker, P. R. Silver Ink Formulations for Sinter-free Printing of Conductive Films. *Sci. Rep.* **2016**, *6*, 20814.
- (23) Mustonen, T.; Kordás, K.; Saukko, S.; Tóth, G.; Penttilä, J. S.; Helistö, P.; Seppä, H.; Jantunen, H. Inkjet Printing of Transparent and Conductive Patterns of Single-Walled Carbon Nanotubes and PEDOT-PSS Composites. *Phys. Status Solidi B* **2007**, *244*, 4336–4340.
- (24) Kumar, S. K.; Benicewicz, B. C.; Vaia, R. A.; Winey, K. I. 50th Anniversary Perspective: Are Polymer Nanocomposites Practical for Applications? *Macromolecules* **2017**, *50*, 714–731.
- (25) Barrau, S.; Demont, P.; Peigney, A.; Laurent, C.; Lacabanne, C. DC and AC Conductivity of Carbon Nanotubes–Polyepoxy Composites. *Macromolecules* **2003**, *36*, 5187–5194.
- (26) Bello, A.; Laredo, E.; Marval, J. R.; Grima, M.; Arnal, M. L.; Müller, A. J.; Ruelle, B.; Dubois, P. Universality and Percolation in Biodegradable Poly( $\epsilon$ -caprolactone)/Multiwalled Carbon Nanotube Nanocomposites from Broad Band Alternating and Direct Current Conductivity at Various Temperatures. *Macromolecules* **2011**, *44*, 2819–2828.
- (27) Tchoul, M. N.; Ford, W. T.; Ha, M. L. P.; Chavez-Sumarriva, I.; Grady, B. P.; Lolli, G.; Resasco, D. E.; Areppali, S. Composites of Single-Walled Carbon Nanotubes and Polystyrene: Preparation and Electrical Conductivity. *Chem. Mater.* **2008**, *20*, 3120–3126.
- (28) Li, J.; Ma, P. C.; Chow, W. S.; To, C. K.; Tang, B. Z.; Kim, J.-K. Correlations between Percolation Threshold, Dispersion State, and Aspect Ratio of Carbon Nanotubes. *Adv. Funct. Mater.* **2007**, *17*, 3207–3215.
- (29) Yoonessi, M.; Gaier, J. R. Highly Conductive Multifunctional Graphene Polycarbonate Nanocomposites. *ACS Nano* **2010**, *4*, 7211–7220.
- (30) Stankovich, S.; Dikin, D. A.; Domke, G. H. B.; Kohlhaas, K. M.; Zimney, E. J.; Stach, E. A.; Piner, R. D.; Nguyen, S. T.; Ruoff, R. S. Graphene-Based Composite Materials. *Nature* **2006**, *442*, 282–286.
- (31) Qi, X.-Y.; Yan, D.; Jiang, Z.; Cao, Y.-K.; Yu, Z.-Z.; Yavari, F.; Koratkar, N. Enhanced Electrical Conductivity in Polystyrene Nanocomposites at Ultra-Low Graphene Content. *ACS Appl. Mater. Interfaces* **2011**, *3*, 3130–3133.
- (32) Li, W.; Tang, X.-Z.; Zhang, H.-B.; Jiang, Z.-G.; Yu, Z.-Z.; Du, X.-S.; Mai, Y.-W. Simultaneous Surface Functionalization and Reduction of Graphene Oxide with Octadecylamine for Electrically Conductive Polystyrene Composites. *Carbon* **2011**, *49*, 4724–4730.
- (33) Kudin, K. N.; Ozbas, B.; Schniepp, H. C.; Prud'homme, R. K.; Aksay, I. A.; Car, R. Raman Spectra of Graphite Oxide and Functionalized Graphene Sheets. *Nano Lett.* **2008**, *8*, 36–41.
- (34) Daulton, T. L.; Pinter, N.; Scott, A. C. No Evidence of Nanodiamonds in Younger-Dryas Sediments to Support an Impact Event. *Proc. Natl. Acad. Sci. U.S.A.* **2010**, *107*, 16043–16047.
- (35) Dato, A.; Radmilovic, V.; Lee, Z.; Phillips, J.; Frenklach, M. Substrate-Free Gas-Phase Synthesis of Graphene Sheets. *Nano Lett.* **2008**, *8*, 2012–2016.
- (36) Vaia, R. A.; Giannelis, E. P. Lattice Model of Polymer Melt Intercalation in Organically-Modified Layered Silicates. *Macromolecules* **1997**, *30*, 7990–7999.
- (37) Yoonessi, M.; Toghiani, H.; Daulton, T. L.; Lin, J.-S.; Pittman, C. U., Jr. Clay Delamination in Clay/Poly(Dicyclopentadiene) Nanocomposites Quantified by Small Angle Neutron Scattering and

- High-Resolution Transmission Electron Microscopy. *Macromolecules* **2005**, *38*, 818–831.
- (38) Ramanathan, T.; Abdala, A. A.; Stankovich, S.; Dikin, D. A.; Herrera-Alonso, M.; Piner, R. D.; Adamson, D. H.; Schniepp, H. C.; Chen, X.; Ruoff, R. S.; Nguyen, S. T.; Aksay, I. A.; Prud'Homme, R. K.; Brinson, L. C. Functionalized Graphene Sheets for Polymer Nanocomposites. *Nat. Nanotechnol.* **2008**, *3*, 327–331.
- (39) Zabihi, O.; Ahmadi, M.; Abdollahi, T.; Nikafshar, S.; Naebe, M. Collision-Induced Activation: Towards Industrially Scalable Approach to Graphite Nanoplatelets Functionalization for Superior Polymer Nanocomposites. *Sci. Rep.* **2017**, *7*, 3560.
- (40) Yoonessi, M.; Dittler, M.; Peck, J.; Gaier, J. A. Controlled direction of electrical and mechanical properties in nickel tethered graphene polyimide nanocomposites using magnetic field. *Carbon* **2015**, *84*, 375–382.
- (41) Sahimi, M. *Applications of Percolation Theory* London; Taylor and Francis: London, 1994.
- (42) Sahimi, M. Relation Between the Critical Exponent of Elastic Percolation Networks and the Conductivity and Geometrical Exponents. *J. Phys. C: Solid State Phys.* **1986**, *19*, L79.
- (43) Sahimi, M.; Hughes, B. D.; Scriven, L. E.; Davis, H. T. Critical Exponent of Percolation Conductivity by Finite-Size Scaling. *J. Phys. C: Solid State Phys.* **1983**, *16*, L521–L527.
- (44) Sahimi, M.; Hughes, B. D.; Scriven, L. E.; Davis, H. T. Stochastic Transport in Disordered Systems. *J. Chem. Phys.* **1983**, *78*, 6849–6864.
- (45) Halperin, B. I.; Feng, S.; Sen, P. N. Differences between Lattice and Continuum Percolation Transport Exponents. *Phys. Rev. Lett.* **1985**, *54*, 2391–2394.
- (46) Sahimi, M. *Heterogeneous Materials I*; Springer: New York, 2003.
- (47) Varenik, M.; Green, M. J.; Regev, O. Distinguishing Self-Assembled Pyrene Structures from Exfoliated Graphene. *Langmuir* **2016**, *32*, 10699–10704.
- (48) Bon, S. B.; Valentini, L.; Moustafa, R. M.; Jradi, F. M.; Kaafarani, B. R.; Verdejo, R.; Lopez-Manchado, M. A.; Kenny, J. M. Morphology and Photoelectrical Properties of Solution Processable Butylamine-Modified Graphene- and Pyrene-Based Organic Semiconductor. *J. Phys. Chem. C* **2010**, *114*, 11252–11257.
- (49) Alam, A.; Meng, Q.; Shi, G.; Arabi, S.; Ma, J.; Zhao, N.; Kuan, H.-C. Electrically Conductive, Mechanically Robust, PH-Sensitive Graphene/Polymer Composite Hydrogels. *Compos. Sci. Technol.* **2016**, *127*, 119–126.
- (50) Liao, K.-H.; Qian, Y.; Macosko, C. W. Ultralow Percolation Graphene/Polyurethane Acrylate Nanocomposites. *Polymer* **2012**, *53*, 3756–3761.
- (51) Nassira, H.; Sánchez-Ferrer, A.; Adamcik, J.; Handschin, S.; Mahdavi, H.; Qazvini, N. T.; Mezzenga, R. Gelatin–Graphene Nanocomposites with Ultralow Electrical Percolation Threshold. *Adv. Mater.* **2016**, *28*, 6914–6920.
- (52) Hicks, J.; Behnam, A.; Ural, A. A Computational Study of Tunneling-Percolation Electrical Transport in Graphene-Based Nano-composites. *Appl. Phys. Lett.* **2009**, *95*, 213103.
- (53) Balberg, I.; Anderson, C. H.; Alexander, S.; Wagner, N. Excluded Volume and Its Relation to the Onset of Percolation. *Phys. Rev. B: Condens. Matter Mater. Phys.* **1984**, *30*, 3933–3943.
- (54) Delaney, G. W.; Cleary, P. W. The Packing Properties of Superellipsoids. *EPL* **2010**, *89*, 34002.
- (55) Sheng, P.; Sichel, E. K.; Gittleman, J. I. Fluctuation-Induced Tunneling Conduction in Carbon-Polyvinylchloride Composites. *Phys. Rev. Lett.* **1978**, *40*, 1197–1200.
- (56) Linares, A.; Canalda, J. C.; Cagiao, M. E.; García-Gutiérrez, M. C.; Nogales, A.; Martín-Gullón, I.; Vera, J.; Ezquerra, T. A. Broad-Band Electrical Conductivity of High Density Polyethylene Nanocomposites with Carbon Nanoadditives: Multiwall Carbon Nanotubes and Carbon Nanofibers. *Macromolecules* **2008**, *41*, 7090–7097.
- (57) Kilbride, B. E.; Coleman, J. N.; Fraysse, J.; Fournet, P.; Cadek, M.; Drury, A.; Hutzler, S.; Roth, S.; Blau, W. J. Experimental Observation of Scaling Laws for Alternating Current and Direct Current Conductivity in Polymer-Carbon Nanotube Composite Thin Films. *J. Appl. Phys.* **2002**, *92*, 4024–4030.
- (58) Jonscher, A. K. The “Universal” Dielectric Response. *Nature* **1977**, *267*, 673–679.
- (59) Weng, W.; Chen, G.; Wu, D. Transport Properties of Electrically Conducting Nylon 6/Foliated Graphite Nanocomposites. *Polymer* **2005**, *46*, 6250–6257.
- (60) Connor, M. T.; Roy, S.; Ezquerra, T. A.; Calleja, F. J. B. Broadband ac Conductivity of Conductor-Polymer Composites. *Phys. Rev. B* **1998**, *57*, 2286.